

# Assessment of exchange-correlation functionals for the calculation of dynamical properties of small clusters in TDDFT

M. A. L. Marques<sup>\*†</sup>, Alberto Castro<sup>\*</sup> and Angel Rubio<sup>‡\*</sup>

<sup>\*</sup>*Departamento de Física Teórica, Universidad de Valladolid, E-47011 Valladolid, Spain*

<sup>†</sup>*Centro de Física Computacional, Departamento de Física da Universidade de Coimbra, Rua Larga, 3004-516, Coimbra, Portugal*

<sup>‡</sup>*Laboratoire de Solides Irradiés (LSI), CNRS-CEA, École Polytechnique, F-91128 Palaiseau, France and*

*Donostia International Physics Center (DIPC), 20018 San Sebastian (Spain)*

(December 2, 2024)

## Abstract

We present a detailed study of different exchange-correlation (xc) functionals in describing the dynamical properties of finite systems. For that purpose, we calculated the static polarizabilities, ionization potentials and optical absorption spectrum of four small clusters, Na<sub>2</sub>, Na<sub>4</sub>, SiH<sub>4</sub> and Si<sub>2</sub>H<sub>6</sub>, using a real-space, real-time technique. The computed static polarizabilities and ionization potentials seem to be in rather good agreement with the available experimental data, once the proper asymptotics of the potential are taken into account. The same conclusion holds for the absorption spectra, although the xc kernels in use do not provide a sufficiently strong attractive interaction between electrons and holes, leading to spectra slightly shifted towards higher energies. This deficiency is traced back to the insufficient description of dynamical effects in the correlation functional. Furthermore, it is shown that the xc potential used to obtain the ground state is the key factor to get reasonable spectra, whereas the choice of the xc kernel just amounts to small, although important, quantitative changes.

## I. INTRODUCTION

Density Functional Theory (DFT) [1] became, in the two last decades, the method of election for the *ab initio* calculation of material properties. Systems with a couple thousand atoms are now routinely investigated, and the calculated energies, geometries, etc., very often agree spectacularly with the experimental data. This success, however, was not immediate: More than twenty years of research were necessary to obtain an exchange-correlation (xc)

---

<sup>\*</sup>On sabbatical leave from Departamento de Física Teórica, Universidad de Valladolid, E-47011 Valladolid, Spain

energy functional which was precise enough to satisfy the quantum-chemistry needs. The accurate and sophisticated Generalized Gradient Approximations (GGA) that we now have at our disposal are indeed the result of a long history of attempts, tests and failures.

Despite these remarkable achievements, there are some quantities which are beyond the reach of the conventional DFT theory. In this Article we will be concerned by one of such properties, namely electronic excitation energies and optical spectra. Several extensions of the original framework were put forward to obtain excited-state properties. From all different approaches, Time-Dependent DFT (TDDFT) [2] emerged the last years as the main DFT formalism for these calculations. One of the main advantages of the TDDFT formulation is that it allows one to deal with problems beyond the perturbative regime as, for example, the response of atoms to ultra-short and intense laser beams. In this way, by solving the time-dependent Kohn-Sham (KS) equations, we can get, *e.g.*, information concerning the harmonic spectrum or the ionization yields. This type of approach is very important in condensed matter science where femtosecond laser pulses are used to monitor the dynamics of electrons in a solid. Furthermore, with larger computational power, we may deal with non-adiabatic couplings between the electronic and the ionic degrees of freedom in presence of these high electromagnetic fields (we may observe phonon assisted structural transformation induced by these external fields).

Excitation energies can be obtained from TDDFT either from the position of the poles of the KS linear response function [3,4], or from the time-dependent density. In the second case, we will be using an approximated xc time-dependent potential,  $v_{xc}(\mathbf{r}, t)$ , while in the former, the key quantity is the xc kernel,  $f_{xc}(\mathbf{r}, \mathbf{r}', t, t')$ , defined by the functional derivative:

$$f_{xc}(\mathbf{r}, \mathbf{r}', t, t') = \frac{\delta v_{xc}(\mathbf{r}, t)}{\delta n(\mathbf{r}', t')}. \quad (1)$$

As expected, the xc kernel, due to its complicated structure, is much harder to model than the local time-dependent xc potential. Furthermore, both calculations usually start from the KS ground-state of the system, which depends on the approximation used for the static  $v_{xc}(\mathbf{r})$ .

One of the most widely used approximation to time-dependent phenomena is the adiabatic local density approximation (ALDA). Although this functional is constructed using the xc correlation energy of the (constant density) electron gas, it yields, like the LDA does in the static case, rather accurate results for systems with rapidly varying densities, as atoms, surfaces or clusters [5–8]. For example, the photo-absorption spectrum of rare-atom gases was computed in Ref. [6] and the agreement with experiment is remarkably good. Results of similar quality have been achieved for the photo-response of small metallic and semiconducting clusters [7]. For the metallic clusters it was shown that the inclusion of xc effects in the dielectric response was important to get the correct red-shift, as compared to experiments, while for the semiconducting (silicon) clusters it was found that the spectra of different isomers was sufficiently different to distinguish between them. Surface and confinement effects were responsible for the appearance of absorption in the optical range for the two silicon clusters,  $\text{Si}_4$  and  $\text{Si}_6$ . Similar results were found for  $\text{C}_{20}$  clusters [9].

The purpose of this work is twofold: To address the impact of a good xc-potential in the optical spectrum of small clusters and to estimate how relevant the  $f_{xc}$  kernel is in this respect. We note that in Ref. [4] the quality of different functionals was tested for light

atoms, and in Ref. [10] for the calculation of the correlation energy of the homogeneous electron gas. In the first of these works, which included calculations using the exact static xc potential, the correct description of the xc-potential used to obtain the ground state seemed to be the dominant factor, whereas the kernel played a marginal role. However this was not the case when looking at the total correlation energy of the homogeneous electron gas. In particular, the nonzero spatial range of  $f_{xc}(r, r', \omega)$  could not be neglected, whereas the frequency dependence appeared to be less important. Our work clearly demonstrates that the optical spectrum of small systems is not only determined by the static xc potential, but also the kernel plays a role.

The rest of the Article is structured in the following way: In Section II, we give a brief overview of the xc functional zoo used in static KS calculations; We then proceed by explaining how these functionals can be changed in order to be used in TDDFT calculations; In Section IV we give some details on the techniques used in our calculations, and present our results for some selected sodium and silicon clusters; We finally conclude and give some remarks on the quality of the functionals tested.

## II. XC FUNCTIONALS FOR STATIC DFT

The first (and simplest) approximation for the xc functional, the Local Density Approximation (LDA) introduced by Kohn and Sham in 1965 [11], yielded remarkably good results for such a modest effort, but the method didn't prove accurate enough to be used in theoretical chemistry. The LDA xc energy functional can be written as

$$E_{xc}^{LDA} = \int d^3\mathbf{r} n(\mathbf{r}) \epsilon_{xc}^{\text{hom}}(n(\mathbf{r})), \quad (2)$$

where  $n(\mathbf{r})$  is the electronic density at point  $\mathbf{r}$ , and  $\epsilon_{xc}^{\text{hom}}(n)$  stands for the xc energy density of the homogeneous electron gas with density  $n$ . This function is calculated very accurately using Monte-Carlo techniques [12], and then fitted to some simple analytical function [13]. The functional (2) has several shortcomings, among which we point out the following:

- It neglects non-local effects, *i.e.* the LDA xc energy density at point  $\mathbf{r}$  only depends on the density at that point. We therefore should not expect this functional to work in cases where the density has very strong spatial variations.
- The exchange part of the functional does not cancel exactly the self-energy part of the Hartree term. This leads to a wrong asymptotic behavior of the xc potential for finite systems (it goes exponentially to zero, instead as  $-e^2/r$ ). Properties that strongly depend on this asymptotic behavior, like the ionization potential of atoms and molecules, come out with very large errors. Also, there are no Rydberg states within the LDA, and negative ions usually do not bind, which renders the calculation of electron-affinities impossible.
- LDA usually overbinds, giving too short bond-lengths, etc.

The next generation of functionals included the so-called Generalized Gradient Approximated (GGA) functionals [14–16]. They can be written as:

$$E_{\text{xc}}^{\text{GGA}} = \int d^3\mathbf{r} n(\mathbf{r}) \epsilon_{\text{xc}}^{\text{GGA}}(n(\mathbf{r}), \nabla n(\mathbf{r})), \quad (3)$$

where  $\nabla n(\mathbf{r})$  is the gradient of the density at the point  $\mathbf{r}$ .  $\epsilon_{\text{xc}}^{\text{GGA}}$  is usually some analytic function with some free parameters that are either fitted to experiment, or determined by some exact sum-rules. GGAs solve some of the problems present in the LDA, and in some cases yield results with high enough precision to be used as a tool in quantum chemistry calculations. Recently, a new class of functionals generalizing the GGAs has been proposed. These so-called Meta-GGAs [17], depend explicitly not only on the density and its gradient, but also on the kinetic energy density<sup>1</sup>. This extra dependence adds more flexibility, and allows better approximations to the exact xc functional to be built. Unfortunately, all the GGAs and MGGAs proposed till now suffer, to different degrees, from the same self-interaction problem as the original LDA. A way to circumvent it was proposed by van Leeuwen and Baerends in 1994 [18]: They applied Becke's construction [14] not to the derivation of the exchange energy functional (like in Becke's original work), but to the modeling of the exchange potential directly. By imposing the correct asymptotic behavior to the exchange potential, they were able to get much better ionization potentials (and eigenvalues in general). The price to pay is a much lower precision in the energy, which has to be calculated from the Levy-Perdew formula [19].

To complete the zoo of energy functionals, we still have to refer to orbital functionals, in the so-called Optimized Effective Potential (OEP), or Optimized Potential Method (OPM) [20]. This third generation of functionals is written explicitly in terms of the Kohn-Sham orbitals (being nevertheless implicit functionals of the density):

$$E_{\text{xc}}^{\text{OEP}} = E_{\text{xc}}^{\text{OEP}} [\varphi_1(\mathbf{r}) \cdots \varphi_N(\mathbf{r})]. \quad (4)$$

The xc potential is then calculated using twice the chain-rule for functional derivatives:

$$\begin{aligned} v_{\text{xc}}^{\text{OEP}}(\mathbf{r}) &= \frac{\delta E_{\text{xc}}^{\text{OEP}}}{\delta n(\mathbf{r})} \\ &= \sum_{i=1}^N \int d^3\mathbf{r}' d^3\mathbf{r}'' \left[ \frac{\delta E_{\text{xc}}^{\text{OEP}}}{\delta \varphi_i(\mathbf{r}')} \frac{\delta \varphi_i(\mathbf{r}')}{\delta v_{\text{KS}}(\mathbf{r}'')} + \text{c.c.} \right] \frac{\delta v_{\text{KS}}(\mathbf{r}'')}{\delta n(\mathbf{r})}. \end{aligned} \quad (5)$$

The first term of the right,  $\frac{\delta E_{\text{xc}}^{\text{OEP}}}{\delta \varphi_i(\mathbf{r}'')}$ , can easily be obtained from the expression for  $E_{\text{xc}}^{\text{OEP}} [\varphi_1(\mathbf{r}) \cdots \varphi_N(\mathbf{r})]$ , while the second,  $\frac{\delta \varphi_i(\mathbf{r}')}{\delta v_{\text{KS}}(\mathbf{r}'')}$  can be calculated using first-order perturbation theory. Finally, the remaining functional derivative can be identified with the inverse of the response function for non-interacting electrons,  $\chi_{\text{KS}}^{-1}(\mathbf{r}, \mathbf{r}')$ . Rearranging the terms in Eq. (5), we obtain an integral equation for  $v_{\text{xc}}^{\text{OEP}}$ . The solution of this integral equation is numerically very involved, and has only been achieved for systems with very high symmetry. An alternative is to perform an approximation first proposed by Krieger, Lee and Iafrate [21] (KLI), which transforms the hard task of solving an integral equation in three dimensional space into the simple one of solving a small set of linear equations.

---

<sup>1</sup> The MGGAs, due to the explicit dependence on the kinetic energy density are, in fact, not simple GGAs, but orbital functionals.

Two examples of these orbital functionals are the exact exchange (EXX), and self-interaction corrected (SIC) LDA functionals [13]. In the first, one employs the exact expression for the exchange energy:

$$E_x^{\text{EXX}} = -\frac{1}{2} \sum_{\sigma} \sum_{i,j=1}^N \int d^3\mathbf{r} d^3\mathbf{r}' \frac{\varphi_{j\sigma}^*(\mathbf{r}) \varphi_{i\sigma}^*(\mathbf{r}') \varphi_{i\sigma}(\mathbf{r}) \varphi_{j\sigma}(\mathbf{r}')}{|\mathbf{r} - \mathbf{r}'|}. \quad (6)$$

The SIC-LDA functional, originally proposed by Perdew and Zunger [13], can be written as:

$$E_{\text{xc}}^{\text{SIC}} = E_{\text{xc}}^{\text{LDA}} [n_{\uparrow}(\mathbf{r}), n_{\downarrow}(\mathbf{r})] - \sum_{\sigma} \sum_{i=1}^N E_{\text{xc}}^{\text{LDA}} [|\varphi_i(\mathbf{r})|^2, 0] - \frac{1}{2} \sum_{\sigma} \sum_{i=1}^N \frac{|\varphi_{i\sigma}(\mathbf{r})|^2 |\varphi_{i\sigma}(\mathbf{r}')|^2}{|\mathbf{r} - \mathbf{r}'|}. \quad (7)$$

It is clear that the SIC-LDA obeys two of the features of the exact functional: It exactly cancels the self-interaction part of the Hartree energy and it vanishes for one electron systems. The SIC-LDA functional is nevertheless ill-defined, for it is not invariant upon an unitary transformation of the Kohn-Sham wave-functions.

### III. XC FUNCTIONALS FOR TDDFT

The simplest, and most commonly used, approximation to the xc functional in TDDFT is the adiabatic LDA (ALDA), in which the static LDA functional is used for the dynamical properties, but evaluated at the time-dependent density:

$$v_{\text{xc}}^{\text{ALDA}}(\mathbf{r}, t) = v_{\text{xc}}^{\text{hom}}(n(\mathbf{r}, t)). \quad (8)$$

In the ALDA, the  $f_{\text{xc}}$  kernel is a contact function in time and space:

$$f_{\text{xc}}^{\text{ALDA}}(\mathbf{r}, t; \mathbf{r}', t') = \delta(t - t') \delta(\mathbf{r} - \mathbf{r}') \left. \frac{dv_{\text{xc}}^{\text{hom}}(n)}{dn} \right|_{n=n(\mathbf{r}, t)}. \quad (9)$$

Following the same reasoning, it is straightforward to write adiabatic GGA potentials and  $f_{\text{xc}}$  kernels. Unfortunately, the thresholds for the onset of absorption calculated either with adiabatic LDA or GGA functionals are typically below the observed ones (by several eV in the case of atoms). This is an intrinsic drawback of the ALDA/GGA because, in principle, TDDFT should yield the correct thresholds. This problem is once more related to the wrong asymptotic behavior of the effective Kohn-Sham potential that goes exponentially to zero instead of  $-e^2/r$  for neutral systems. This is due, as already mentioned in the previous Section, to the insufficient correction of the self-interaction part of the Hartree potential. Also the xc kernel,  $f_{\text{xc}}$ , suffers from a self-interaction error. Non-local approximations to the xc potential retaining the correct asymptotic behavior improve the response properties of metal clusters.

A generalization of the EXX potential to the time-domain is also possible [22]. It starts from the perturbative expansion of the action functional and then uses the chain-rule for

functional derivatives to derive an integral equation for the xc potential. A KLI-like approximation can then be used to simplify the task of solving this integral equation. Using the same procedure, one can derive an integral equation for  $f_{xc}$ . However, for practical calculations, it is desirable to devise a simple analytical expression for the xc kernel. To this end, it is common practice to further simplify the KLI potential by neglecting one of its terms [22]. In the static exchange-only case, this leads to the so-called Slater approximation [23].  $f_{xc}$  then reads:

$$f_{xc}^{\text{EXX approx.}}(\mathbf{r}t, \mathbf{r}'t') = -\delta(t - t')\delta_{\sigma\sigma'} \frac{\left| \sum_{i=1}^N \varphi_{i\sigma}(\mathbf{r})\varphi_{i\sigma}^*(\mathbf{r}') \right|^2}{|\mathbf{r} - \mathbf{r}'| n_{\sigma}(\mathbf{r})n_{\sigma}(\mathbf{r}')}. \quad (10)$$

One should note that, due to the extra functional derivative in the definition of the xc kernel, it is much more complicated, in this case, to evaluate directly  $f_{xc}$  than to time-propagate the KS states with  $v_{xc}$ .

Finally, an adiabatic SIC-LDA can be easily written in the spirit of Eq. (7).

#### IV. METHOD AND RESULTS

We used a real-space, real-time approach to solve the TD Kohn-Sham equations for  $\text{Na}_2$ ,  $\text{Na}_4$ , silane ( $\text{SiH}_4$ ) and disilane ( $\text{Si}_2\text{H}_6$ ). This time-evolution method is adequate to be combined with real-space calculations of the ground-state by means of the finite-difference pseudopotential method [24,25], or with adaptative coordinates [26]. In both cases, a real-space discretization of the kinetic energy operator leads to sparse Hamiltonian matrices which do not need to be stored in memory, and are easy to handle. Furthermore, in order to propagate the states in time, we do not need to compute the complicated  $f_{xc}$  kernel, but only the much simpler  $v_{xc}$  potential. In this way, we are able to do time-dependent EXX calculations *without* having to perform Slater's approximation [22,23].

The space was uniformly discretized, with mesh-spacing ranging from 0.4Å for the sodium clusters to 0.25Å for the silicon ones, and the points were contained inside a sphere with radius 10Å for sodium and 7Å for silicon. The ionic potential was modeled by a soft-core Troullier-Martins pseudopotential [27]. By using these settings, a convergence of better than 0.1 eV was reached for the eigenvalues. The time-evolution was performed with a modified Krank-Nicholson rule, with a time-step of 0.0025  $\hbar/\text{eV}$ , for a total evolution time,  $T_{max}$ , of 50  $\hbar/\text{eV}$  for the sodium clusters and 25  $\hbar/\text{eV}$  for the silicon clusters. With this parameters we can resolve excitation energies within  $\Delta E = 2\pi\hbar/T_{max}$  that corresponds to tenths of eV. We added absorbing boundary conditions to improve the quality of the spectrum above the ionization threshold (avoiding artificial formation of standing waves in the spherical box used to confine the cluster).

To calculate the dipole strength function (which is simply proportional to the absorption cross-section), we prepare our system in the ground-state, and then excite it with a delta electric field,  $E_0\delta(t)$ . The dipole strength can then be related to the imaginary part of the dynamical polarizability:

$$S(\omega) = \frac{4\pi m_e}{h^2} \omega \Im \alpha(\omega), \quad (11)$$

where  $h$  is Planck's constant,  $m_e$  the electron's mass, and the dynamical polarizability,

$$\alpha(\omega) = -\frac{2}{E_0} \int dr z \delta n(\mathbf{r}, \omega). \quad (12)$$

In the last expression,  $\delta n(\mathbf{r}, \omega)$  stands for the Fourier transform of  $n(\mathbf{r}, t) - n(\mathbf{r}, t = 0)$ . The calculation of the dipole strength involves two important approximations: The choice of the static xc potential used to obtain the ground-state, and the time-dependent xc potential (directly related to the  $f_{xc}$  kernel) used to propagate the state. The relative importance of both is still fairly obscure. Petersilka et al. linear-response results [4] for the Helium and Beryllium atoms indicates that the choice of the  $f_{xc}$  kernel is less dramatic than the choice of a good static  $v_{xc}$  potential. However, this is no longer true for the lowest excitation energies of Beryllium and if we look at the singlet-triplet splittings, where the effects arising from  $v_{xc}$  cancel. The fairly accurate results of Lithium and Beryllium within the LDA were related to the quality of the ground state calculation for few electron systems as light atoms and the  $H_2$  molecule [28].

By performing the time evolution, in the limit  $t \rightarrow \infty$ , we have all the information about the linear response of the system, and should therefore be able to study the xc kernel *without* having to perform explicitly the functional derivative of the xc potential. Thus, we can study the effect of different  $f_{xc}$  kernels for a fixed  $v_{xc}$  potential in the time-evolution method. To address this question, we propose the following method: First, we obtain the ground state of the system with the static functional  $v_{xc}^{(1)}$ , and then perform the time evolution with the xc potential:

$$v_{xc}(\mathbf{r}, t) = v_{xc}^{(1)}(\mathbf{r}, t = 0) + [v_{xc}^{(2)}(\mathbf{r}, t) - v_{xc}^{(2)}(\mathbf{r}, t = 0)], \quad (13)$$

where  $v_{xc}^{(2)}$  is some other xc functional. In this way, we probe the importance of the  $f_{xc}^{(2)}$  kernel, without having to spend more computational time in calculating this rather complex quantity. This method will be used for silane, for a varied selection of  $v_{xc}^{(1)}$  and  $v_{xc}^{(2)}$  to quantify the dependence of the dynamical spectrum with the xc-potential and kernel.

In the following, PZ stands for LDA [11], with  $\epsilon_c^{\text{hom}}$  taken from Monte-Carlo calculations [12] and then parametrized by Perdew and Zunger [13]; PBE is the Perdew, Becke and Ernzerhof GGA functional [16]; LB94 represents the van Leeuwen and Baerends exchange potential [18], to which we sum the PBE correlation potential; SIC is the SIC-LDA functional [13]; and, finally, EXX stands for exact-exchange [22]. SIC and EXX are both treated within the KLI approximation [21]. "exp" will be used to denote experimental values. All energies are measured in eV unless otherwise stated.

## A. Sodium

In Table I we show the ionization potentials (IP), obtained from the highest occupied KS eigenvalue, and HOMO-LUMO gap for the two sodium clusters. The IPs obtained either by using the LDA or the GGA functionals are much smaller than the experimental value. This is a well known problem related to the wrong asymptotic behavior of the potentials. The situation does improve enormously for  $\text{Na}_2$  if we correct for this deficiency, as can be seen from the LB94, SIC and EXX values. For  $\text{Na}_4$ , these functionals overestimate the IP by more

than 0.6 eV. Although the calculated IPs differ by more than 2 eV, the HOMO-LUMO gap stays essentially constant, *i.e.*, correcting for the asymptotic part of the exchange potential amounts to a constant shift in the eigenvalues, and not to an opening of the gap.

All the calculated optical spectra for Na<sub>2</sub> are quite similar (see Fig. 1), regardless of the xc potential used, and exhibit three clear peaks in the 2-5 eV range (the third peak in the LB94 curve is almost completely smeared out). They all compare quite well with experiment, although the DFT peaks are all shifted towards higher energies. This shift can be understood in terms of the competition between the Coulomb repulsion in the electronic kernel and the electron/hole attraction from the xc part of the response (that is,  $\Delta\epsilon = \epsilon_c - \epsilon_v - \langle \varphi_v \varphi_c | \frac{1}{|r_1 - r_2|} | \varphi_v \varphi_c \rangle + \Delta_{xc}$ ). In particular for a given valence-conduction transition  $v \rightarrow c$ , the exchange correlation kernel within the simple ALDA introduced only a local and static *attractive* electron-hole interaction:

$$\Delta_{xc} = \int d^3\mathbf{r}_1 \int d^3\mathbf{r}_2 \varphi_v^*(\mathbf{r}_1) \varphi_c^*(\mathbf{r}_1) \delta(\mathbf{r}_1 - \mathbf{r}_2) \frac{\partial V_{xc}(\mathbf{r}_1)}{\partial n} \varphi_v(\mathbf{r}_2) \varphi_c(\mathbf{r}_2) = \int d^3\mathbf{r}_1 n_1(\mathbf{r}_1) \frac{\partial V_{xc}(\mathbf{r}_1)}{\partial n} n_2(\mathbf{r}_1). \quad (14)$$

This expression is more complicated for the other kernels, but it is clear that they do introduce an effective attractive interaction that it is not complete. We might have to recall that we have neglected dynamical effects and they may need to be included in the xc kernel to recover this minor effect. Also, we should keep in mind that temperature effects (vibrational motion) of the molecule may introduce a broadening of the spectrum as well as a shift of the peaks to lower frequencies [7,29]. The functional which yields the best results for the dimer is, by a small margin, the EXX, while the strongest depart from experiment is the LB94 curve. We note that the 3rd peak in the LDA and PBE spectra lies in the continuum of states (above the ionization threshold). Thus it is more a resonance than a well defined bound transition as observed in experiments [30]. This deficiency is observed in all the clusters studied in the present work and it is, once more, mainly due to the wrong description of the asymptotic part of the exchange potential.

For Na<sub>4</sub> (Fig. 2) all DFT calculations yield very similar spectra (and similar to the many-body results based on a *GW* quasiparticle calculation and including the electron-hole interaction through the solution of the Bethe-Salpeter equation [31]). The spectra consist of three well separated peaks in the 1.5-3.5 eV range, and a broader feature at around 4.5 eV. The comparison with the experimental values is quite good, although the peaks appear, once more, at higher energies. The best results were obtained using the LDA, the GGA or the EXX, while the LB94 spectrum showed the strongest deviation from experiment. Again, the error is larger for the high energy peaks, where transitions to conduction states close to the ionization threshold are involved. Due to the small overlap between these Rydberg-like states and the low-lying states, exchange processes are not relevant and the polarization contribution to correlation, although being generally weak becomes the dominant contribution to the renormalization of these single particle excitations.

Finally, in Table II, we present the static polarizabilities of Na<sub>2</sub> and Na<sub>4</sub>, obtained either through a finite field (static) calculation, or from the Fourier transform of the time-dependent density. For Na<sub>2</sub> all functionals perform equally well, being the results smaller than the experimental value by around 10%. This is consistent with other DFT calculations that give static polarizabilities in the range 33.1-38.2 Å<sup>3</sup> for Na<sub>2</sub> and 67.1-78.7 Å<sup>3</sup> for Na<sub>4</sub>

(see Ref. [32] and results cited therein). In the case of  $\text{Na}_4$ , the orbital functionals SIC and the EXX yield a bit better static polarizabilities than the LDA and the GGAs, but the results are still smaller than the experimental value. We also rejoice that the two methods used to calculate the static polarizability yield very similar results. The neglect of correlation as well as temperature effects is responsible for the obtained smaller polarizabilities values. We indicate that the simple argument that a potential with the correct asymptotic will lead to more localized charge and therefore lower polarizability does not hold for these small systems. These results give support to previous studies on simple metallic jellium spheres [33].

## B. Silicon

We have calculated the two simplest hydrogen terminated silicon clusters: silane ( $\text{SiH}_4$ ) and disilane ( $\text{Si}_2\text{H}_6$ ). These systems pose a much harder challenge than the simple sodium clusters (where even jellium calculations within the LDA yield reasonable results), not only because of the presence of the p-electrons, but also due to the hydrogen, which is very hard to describe by a reasonably soft-core pseudopotential. As expected, the five xc functionals we tried yielded quite dissimilar results.

Our calculations for the IP and HOMO-LUMO gaps for silane and disilane are summarized in Table III. Undoubtedly, EXX and LB94 gave the best IPs of all five functionals tested, almost at the level of the much more involved GW with exciton effects or Monte-carlo calculations. SIC is slightly worse, and LDA and PBE yield, as usual, completely unreal IP. Although the IP changes by more than 4 eV going from the LDA to the EXX, the HOMO-LUMO gap increases by just around 0.5 eV: The main difference is, once more, a nearly rigid shift of the eigenvalues. However, this shift brings once more the relevant single particle transitions below the ionization threshold. This is consistent with the finding that EXX calculations provide larger gaps for semiconductors [34].

We will discuss separately silane and disilane spectra. The silane spectrum (Fig. 3) consists of three peaks between 8 and 12 eV (the two peaks derive from a Jahn-Teller splitting of the triply degenerate  $2t_2 \rightarrow 4s$  transition [35]), followed by a much broader feature at higher energies. The curves obtained with the two traditional functionals, LDA and PBE, are quite similar to each other, and the onset for absorption is underestimated by around 1 eV. The underestimation of the onset of absorption is a well known deficiency of LDA based functionals that is even more dramatic in the case of infinite bulk systems where excitonic effects and band-gap renormalization are not properly described by these simple functionals [36]. The SIC spectrum is unphysically shifted to lower energies (fact that could be anticipated by looking at the low SIC HOMO-LUMO gap), and the first peak is split. This second effect is an artifact of SIC, which, in this implementation, spontaneously breaks the 3-fold degeneracy of the HOMO state. LB94 and EXX behave quite well: the onset for absorption is now correct, and the error in the position of the first three peaks is reduced by a factor of 2 or 3 from the LDA/PBE results (see Table V). van Leeuwen's functional performs marginally better in this case than EXX, which overestimates slightly the excitation energies. The transitions close to the ionization threshold give rise to a peak in the spectrum that in experiments is usually broader than in the calculations, as new decaying channels are available that are not included in the present calculations. Although the functionals we

used do not properly include the damping of the excitations, finite lifetimes can be simulated by convoluting the calculated spectrum with some Lorentzian function.

The disilane LDA, PBE, LB94 and SIC spectra are all very similar (see Fig. 4) and consist of five peaks in the 7-12 eV interval, followed by a broader feature at higher energies. All these curves suffer from the same deficiency: The separation between the second and third peak is too small, so the second peak appears as a shoulder of the third due to the limited resolution of the calculations (in Table V the second line for Si<sub>2</sub>H<sub>6</sub> describes the position of this shoulder). The curve closest to experiment was calculated with the EXX functional (note its first peak at exactly the experimental value). SIC yielded a quite unreasonable spectrum, consisting of broad peaks at too low energies, and consolidated its position of the worst of the five functionals tested (as what concerns the calculation of optical absorption spectra, of course).

For these clusters we also provide the static polarizabilities in Table IV. For silane we find, in agreement with the results for sodium clusters, that all the methods lead to polarizabilities lower than the experimental values. In spite of the proper asymptotics of the EXX functional, LDA yields the best results, which indicates that a subtle error cancellation is taking place, and that it is important to have some sort of correlation in the functional. This result seems to hold true for this small systems and deserves a more detailed analysis.

### C. Xc potential *vs* xc kernel

In order to study the sensitivity of the optical spectra to the xc functional used to calculate the ground-state, and to the time-dependent xc potential used to propagate in time, we plot, in Fig. 5, the spectrum of silane, for some choices of  $v_{xc}^{(1)}$  and  $v_{xc}^{(2)}$  (see Eq. (13)). In the first plot we take ground states calculated with several xc functionals (EXX, LB94 and LDA), and propagate these states with the LDA, while in the second we fix the ground state (calculated with the EXX functional), and use three different potentials to propagate it (LDA, LB94 and EXX). The results clearly indicate that the optical spectrum of SiH<sub>4</sub> is much more sensitive to the choice of the starting state, than to the quality of  $v_{xc}^{(2)}$ . This numerical evidence is in good agreement with the findings of Petersilka et al. [4]. From the second plot of Fig. 5 we see that the ALDA provides the strongest attractive  $f_{xc}$ , shifting the transitions to lower energies by as much as 0.4 eV, the effect being stronger for the high energy transitions. Nevertheless, the role of these functionals needs to be quantified for larger systems and, in particular, for extended systems where the form of the initial potential is expected to be less important and where correlations are supposed to be the dominant contribution to the excitation spectra. This different behavior of finite and infinite systems poses a theoretical problem when designing functionals as the two classes of systems are mainly sensitive either to the spatial non locality or to the frequency dependence of the xc functional.

## V. CONCLUSION

We presented a detailed study of the impact of different xc potentials and kernels in describing the static and dynamical properties of small clusters. The ionization threshold

as well as specific single-particle transitions are very sensitive to the specific form of the xc potential used to obtain the ground state of the system. The static polarizabilities turn out to be rather close to experiment but always smaller than the observed values. Surprisingly, the polarizabilities calculated with the LDA or the GGA are better than the ones calculated with LB94, SIC or EXX. In the case of the EXX, this is related to the absence of dynamical correlations, while the LB94 and the SIC functionals seem to break the subtle error cancellation between exchange and correlation always present in the LDA and the GGA functionals.

For the optical spectra, the opposite conclusion is reached. EXX and LB94 perform remarkably well (although LB94 behaves a bit worse for the sodium clusters), while LDA and GGA show some problems (for example, the onset for optical absorption is underestimated by around 1.5 eV in SiH<sub>4</sub>). SIC performs badly, especially for the silicon clusters. On the other hand, the high lying excitations (below the ionization threshold) are always shifted to higher energies in the EXX and LB94. This error is traced back to the weak effective attractive xc kernels. It seems clear that the right asymptotics of the kernel is important but the missing dynamical contribution (and correlation) is also relevant in order to get a more quantitative agreement with experimental data.

Finally, our spectra calculated with different xc-functional for the ground state calculation and from the time evolution ( $v_{xc}^{(1)} \neq v_{xc}^{(2)}$ ), suggest that the choice xc potential used to calculate the ground state is more important than the choice of the xc kernel for the case of finite systems. This conclusion should not be valid when one is dealing with infinite periodic systems.

## VI. ACKNOWLEDGEMENTS

We benefit from discussions with E. K. U. Gross, G. Bertsch, K. Yabana, L. Reining, and K. Capelle. We acknowledge support by DGES (PB98-0345), JCyL (VA28/99), RTN program of the European Union NANOPHASE (contract HPRN-CT-2000-00167). M. A. L. M. would like to thank the kind hospitality and encouraging discussions with F. Nogueira. A. R. acknowledges the support from the sabbatical program Salvador de Madariaga of the Spanish MEC (PR2000-0335) and the Ecole Polytechnique. A. C. acknowledges the support from the MEC under the graduate fellowship program. Part of the calculations present in this Article were performed at the Centro de Física Computacional of the Universidade de Coimbra.

## REFERENCES

- [1] R. M. Dreizler, and E. K. U. Gross, *Density Functional Theory* (Springer, Berlin, 1990); R. G. Parr, and W. Yang, *Density Functional Theory of Atoms and Molecules* (Oxford University Press, New York, 1989).
- [2] E. Runge, and E. K. U. Gross, Phys. Rev. Lett. **52**, 997 (1984); E. K. U. Gross, J.F. Dobson, and M. Petersilka in *Topics in Current Chemistry* Vol. **181**, 81 (Springer, Berlin, 1196).
- [3] M. Petersilka, U. J. Gossmann, and E. K. U. Gross, Phys. Rev. Lett. **76**, 1212 (1996).
- [4] M. Petersilka, E. K. U. Gross, and K. Burke, 2000, cond-mat/0001154.
- [5] A. Zangwill, and P. Soven, Phys. Rev. A **21**, 1561 (1980).
- [6] M. J. Stott, and E. Zaremba, Phys. Rev. A **21**, 12 (1980); M. E. Casida in *Recent Advances in Density Functional Methods*, Part I, ed. D. P. Chong (World Scientific, Singapore, 1995).
- [7] A. Rubio, J. A. Alonso, X. Blase, L. C. Balbás, and S. G. Louie, Phys. Rev. Lett. **77**, 247 (1996); Phys. Rev. Lett. **77**, E5442 (1996); A. Rubio, J. A. Alonso, X. Blase, and S. G. Louie, Int. J. Mod. Phys. B **11**, 2727 (1996);
- [8] I. Vasiliev, S. Ögüt, and J. R. Chelikowsky, Phys. Rev. Lett. **82**, 1919 (1999).
- [9] A. Castro, M. A. L. Marques, and A. Rubio, (to be published).
- [10] M. Lein, E.K.U. Gross and J.P. Perdew, Phys. Rev. B **61**, 13431 (2000).
- [11] W. Kohn, and L. J. Sham, Phys. Rev. **140**, A1133 (1965).
- [12] D. M. Ceperley and B. J. Alder, Phys. Rev. Lett. **45**, 566 (1980).
- [13] J. P. Perdew, and A. Zunger, Phys. Rev. B **23**, 5048 (1981).
- [14] A. D. Becke, Phys. Rev. A **38**, 3098 (1988);
- [15] C. Lee, W. Yang, R. G. Parr, Phys. Rev. B **37**, 785 (1988).
- [16] J. P. Perdew, K. Burke, and M. Ernzerhof, Phys. Rev. Lett. **77**, 3865 (1996).
- [17] J. P. Perdew, S. Kurth, A. Zupan, and P. Blaha, Phys. Rev. Lett. **82**, 2544 (1999).
- [18] R. van Leeuwen, and E. J. Baerends, Phys. Rev. A **49**, 2421 (1994).
- [19] M. Levy, and J. P. Perdew, Phys. Rev. A **32**, 2010 (1985).
- [20] R. T. Sharp, and G. K. Horton, Phys. Rev. **90**, 317 (1953); J. D. Talman, and W. F. Shadwick, Phys. Rev. A **14**, 36 (1976); C. A. Ullrich, U. J. Gossmann, and E. K. U. Gross, Phys. Rev. Lett. **74**, 872 (1995).
- [21] J. B. Krieger, Y. Li, and G. J. Iafrate, Phys. Rev. A **45**, 101 (1992).
- [22] M. Petersilka, U. J. Gossmann, and E. K. U. Gross, in *Electronic Density Functional Theory: Recent Progress and New Directions*, ed. G. Vignale, J. F. Dobson, and M. P. Das (Plenum Press, New York, 1995)
- [23] J. C. Slater, Phys. Rev. **81**, 385 (1951).
- [24] J. R. Chelikowsky, N. Trouiller, and Y. Saad, Phys. Rev. Lett. **72**, 1240 (1994)
- [25] K. Yabana, and G. F. Bertsch, Phys. Rev. B **54**, 4484 (1996); G. F. Bertsch, J.-I. Iwata, A. Rubio, and K. Yabana, Phys. Rev. B **62**, 7998 (2000); G. F. Bertsch, A. Rubio, and K. Yabana, physics/0003090.
- [26] F. Gygi, and G. Galli, Phys. Rev. B **52**, R2229 (1995); N. A. Modine, G. Zumbach, and E. Kaxiras, Phys. Rev. B **55**, 10289 (1997).
- [27] N. Troullier, and J. L. Martins, Phys. Rev. B **43**, 1993 (1991).
- [28] F. Aryasetiawan, O. Gunnarsson, and A. Rubio, (unpublished)
- [29] J. M. Pacheco, W.-D. Schöne, Phys. Rev. Lett. **79**, 4986 (1997).

- [30] S. P. Sinha, Proc. Phys. Soc. London **62**, 124 (1949); and W. R. Fredrickson, and W. W. Watson, Phys. Rev. **30**, 429 (1927).
- [31] G. Onida, L. Reining, R. W. Godby, R. Del Sole, and W. Andreoni, Phys. Rev. Lett. **75**, 818 (1995).
- [32] S. Kümmel, M. Brack, and P.-G. Reinhard, Phys. Rev. B **62**, 7602 (2000).
- [33] A. Rubio, L.C. Balbás and J.A. Alonso, Phys. Rev. B **45**, 13657 (1992); **46** 4891 (1992).
- [34] M. Stadele, J.A. Majewski, P. Vogl and A. Gorling, Phys. Rev. Lett. **79**, 2089 (1997).
- [35] L. Chantranupong, G. Hirsh, R. J. Buenker, and M. A. Dillon, Chem. Phys. **170**, 167 (1993).
- [36] M. Rohlfing and S. G. Louie, Phys. Rev. Lett. **81**, 2312 (1998); L. X. Benedict, E. L. Shirley, and R. B. Bohn, Phys. Rev. Lett. **80**, 4514 (1998); S. Albrecht, L. Reining, R. Del Sole, and G. Onida, Phys. Rev. Lett. **80**, 4510 (1998).
- [37] A. Herrmann, E. Schumacher, and L. Wöste, J. Chem. Phys. **68**, 2327 (1978).
- [38] D. Rayane, A. R. Allouche, E. Benichou, R. Antoine, M. Aubert-Frecon, Ph. Dugourd, M. Broyer, C. Ristori, F. Chandezon, B. A. Huber, and C. Guet, Eur. Phys. J. D **9**, 243 (1999).
- [39] A. R. Porter, M. D. Towler, and R. J. Needs, unpublished.
- [40] J. C. Grossman, M. Rohlfing, L. Mitas, S. G. Louie, and M. L. Cohen, Phys. Rev. Lett. **86**, 472 (2001).
- [41] B. P. Pullen, T. A. Carlson, W. E. Moddeman, G. K. Schweitzer, W. E. Bull, and F. A. Grimm, J. Chem. Phys. **53**, 768 (1970).
- [42] W. C. Price, *Molecular Spectroscopy, Proc. Conf.* (Institute of Petroleum, London, 1968), p. 221; H. Bock, W. Ensskin, F. Fehér, and R. Freund, J. Am. Chem. Soc. **98**, 668 (1976).
- [43] *The CRC Handbook of Physics and Chemistry, 78th Edition*, ed. D. R. Lide (CRC Press, New York, 1997).
- [44] U. Itoh, Y. Toyoshima, H. Onuki, N. Washida, and T. Ibuki, J. Chem. Phys. **85**, 4867 (1986).
- [45] C. R. C. Wang, S. Pollack, D. Cameron, and M. M. Kappes, J. Chem. Phys. **93**, 3787 (1990).

## TABLE CAPTIONS

Table I: Calculated ionization potentials, (IP), obtained from the highest occupied KS eigenvalue, and HOMO-LUMO gaps for  $\text{Na}_2$  and  $\text{Na}_4$  for different xc functionals compared to available experimental data [37].

Table II: Static polarizabilities for the small sodium clusters estimated using a finite electrical field (FF), or calculated from the  $\omega = 0$  Fourier transform of the time-dependent dipole moment (FT). The results are compared to experiments [38] and other calculations [32].

Table III: Calculated ionization potentials (IP) obtained from the highest occupied KS eigenvalue, and HOMO-LUMO gaps for  $\text{SiH}_4$  and  $\text{Si}_2\text{H}_6$ . The available experimental data as well as results from many body calculations are given for comparison. DMC stands for the diffusion quantum Monte-Carlo calculations of Ref. [39], GW for the GW with exciton effects results (GW-Bethe-Salpeter equation) of Ref. [40], and finally, QMC for quantum Monte-Carlo calculations [40].

Table IV: Static dipolar polarizabilities for the hydrogenated silicon clusters obtained from the  $\omega = 0$  Fourier transform of the time-dependent dipole moment.

Table V: Lowest excitation energies for  $\text{SiH}_4$  and  $\text{Si}_2\text{H}_6$  obtained with different xc-functionals compared to experiments and other calculations based on a many body formalism. The SIC results are absent due to the difficulty to identify the peaks in the spectra. DMC stands for the diffusion quantum Monte-Carlo calculations of Ref. [39], and the calculated value of 9.47 should be compared with the average of the two first, Jahn-Teller splitted, levels. GW are the GW with exciton effects results (GW-Bethe-Salpeter equation) of Ref. [40], and finally, QMC for Quantum Monte-Carlo calculations [40].

## FIGURE CAPTIONS

Fig. 1: Averaged dipole strength for  $\text{Na}_2$ , calculated for several xc functionals. The “exp” curve is from Ref. [8], who adapted the experimental results of Ref. [30]. The experimental curve is plotted in arbitrary units.

Fig. 2: Averaged dipole strength for  $\text{Na}_4$ , calculated for several xc functionals. “exp” stands for the experimental photodepletion cross sections of Ref. [45], while “GW” is the many-body calculation of Ref. [31], which includes self-energy and excitonic effects. These two curves are shown in arbitrary units for the sake of comparison.

Fig. 3: Averaged dipole strength for  $\text{SiH}_4$ , calculated for several xc functionals. The “exp” curve is from Ref. [44].

Fig. 4: Averaged dipole strength for  $\text{Si}_2\text{H}_6$ , calculated for several xc functionals. The “exp” curve is from Ref. [44].

Fig. 5: Averaged dipole strength for  $\text{SiH}_4$ , calculated using different xc-functionals from the calculation of the ground state and for the time evolution ( $v_{\text{xc}}^{(1)} \neq v_{\text{xc}}^{(2)}$ ) (see Eq. 13). For each curve, the first functional mentioned corresponds to  $v_{\text{xc}}^{(1)}$  and the second to  $v_{\text{xc}}^{(2)}$ .

TABLES

TABLE I.

	PZ	PBE	LB94	SIC	EXX	exp [37]
Na <sub>2</sub> IP	3.21	3.22	4.72	5.17	4.76	4.89
Na <sub>2</sub> HOMO-LUMO	1.36	1.36	1.23	1.51	1.45	-
Na <sub>4</sub> IP	3.83	3.82	5.35	5.05	4.89	4.27
Na <sub>4</sub> HOMO-LUMO	1.08	1.07	1.12	1.20	1.01	-

TABLE II.

	PZ	PBE	LB94	SIC	EXX	Ref. [32]	exp
Na <sub>2</sub> FF	35.0	34.3	32.8	33.7	34.9	37.0	39.3
Na <sub>2</sub> FT	34.9	34.1	32.7	33.5	34.7	-	39.3
Na <sub>4</sub> FF	76.7	75.4	74.8	80.0	77.4	78.7	83.8
Na <sub>4</sub> FT	75.9	74.6	73.1	78.6	76.3	-	83.8

TABLE III.

	PZ	PBE	LB94	SIC	EXX	DMC [39]	GW [40]	QMC [40]	exp
SiH <sub>4</sub> IP	8.53	8.55	12.3	11.8	13.1	12.88	12.7	12.6	12.61 [41]
SiH <sub>4</sub> HOMO-LUMO	8.10	8.12	8.34	7.70	8.76	-	13.0	-	-
Si <sub>2</sub> H <sub>6</sub> IP	7.40	7.37	10.8	9.95	10.9	10.90	-	-	10.53-10.7 [42]
Si <sub>2</sub> H <sub>6</sub> HOMO-LUMO	6.76	6.60	6.53	5.98	7.17	-	-	-	-

TABLE IV.

	PZ	PBE	LB94	SIC	EXX	exp [43]
SiH <sub>4</sub>	5.11	4.94	4.79	4.71	4.53	5.44
Si <sub>2</sub> H <sub>6</sub>	9.87	9.58	9.47	10.0	8.70	-

TABLE V.

	PZ	PBE	LB94	EXX	DMC [39]	GW [40]	QMC [40]	exp [44]
SiH <sub>4</sub> 1st	8.23	8.25	8.68	8.93	9.47	9.2	9.1	8.8
SiH <sub>4</sub> 2nd	9.30	9.39	9.72	9.98	-	-	-	9.7
SiH <sub>4</sub> 3rd	10.1	10.1	11.1	11.1	-	-	-	10.7
$\langle \Delta \rangle$	0.52	0.49	0.18	0.27	-	-	-	-
Si <sub>2</sub> H <sub>6</sub> 1st	7.30	7.35	7.36	7.60	-	-	-	7.6
Si <sub>2</sub> H <sub>6</sub> 2nd	8.50	8.60	8.25	8.63	-	-	-	8.4
$\langle \Delta \rangle$	0.20	0.23	0.20	0.12	-	-	-	-

# FIGURES

FIG. 1.

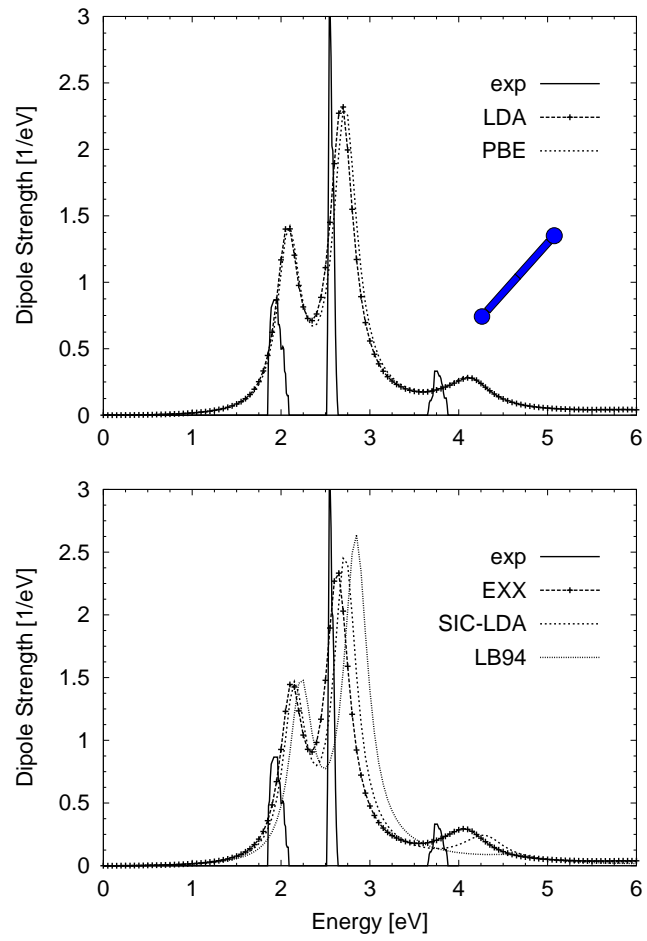


FIG. 2.

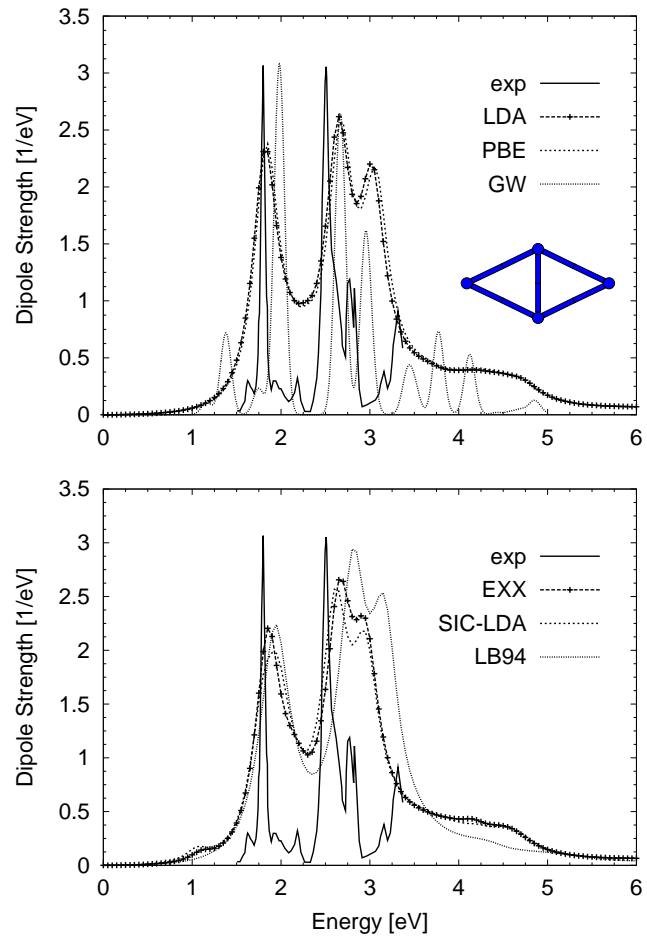


FIG. 3.

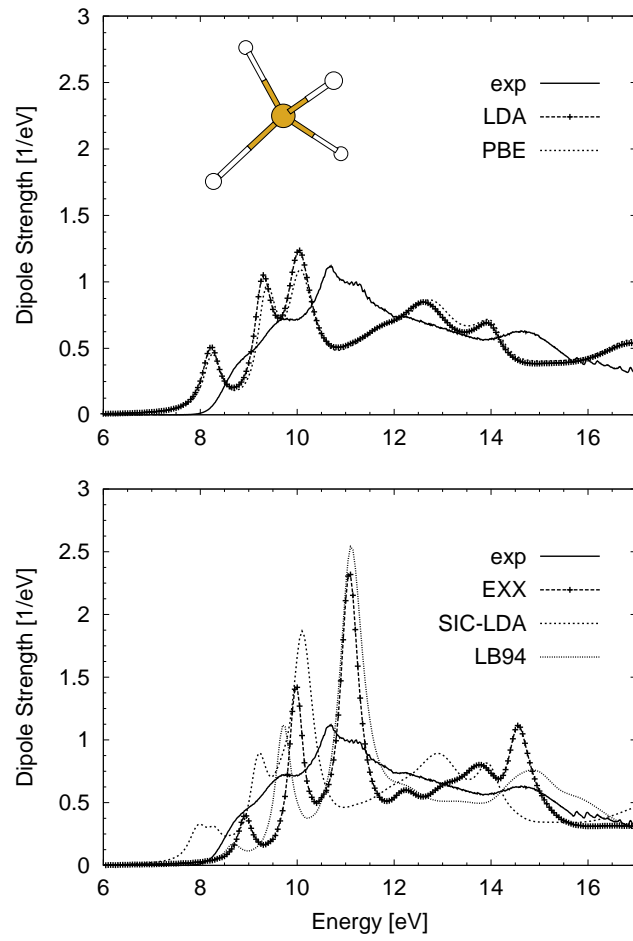


FIG. 4.

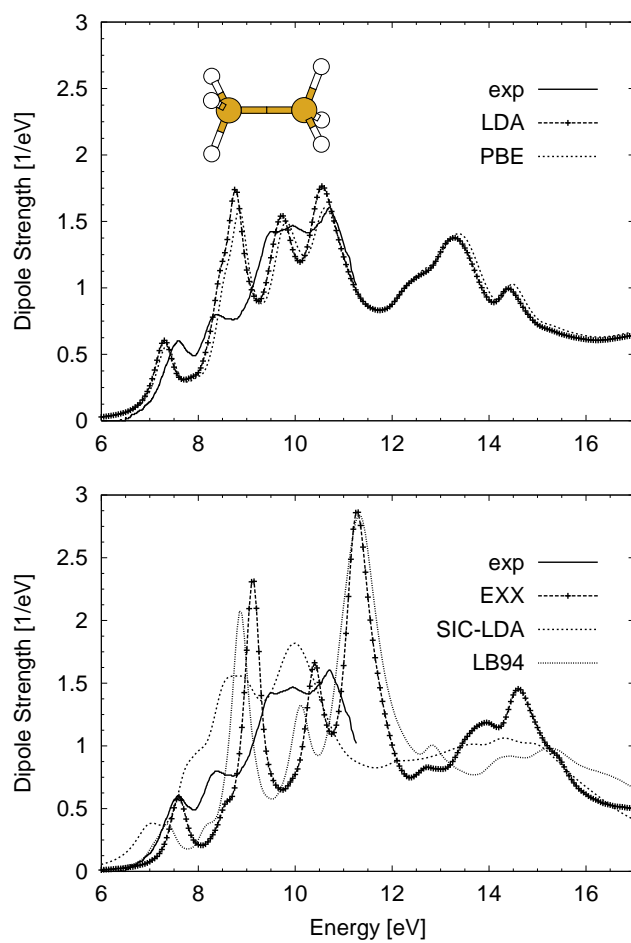


FIG. 5.

